The Fibronectin–ILT3 Interaction Functions as a Stromal Checkpoint that Suppresses Myeloid Cells

Kevin J. Paavola[1], Julie M. Roda[1], Vicky Y. Lin[1], Peirong Chen[1], Kyle P. O'Hollaren[1], Richard Ventura[1], Suzanne C. Crawley[1], Betty Li[1], Hung-I H. Chen[1], Seth Malmersjö[1], Nikolai A. Sharkov[1], Geoffrey Horner[1], Wei Guo[1], Alan K. Kutach[1], Kalyani Mondal[1], Zhen Zhang[1], Joshua S. Lichtman[1], Christina Song[1], Lee B. Rivera[1], Wenhui Liu[1], Jian Luo[1], Yan Wang[1], Mark J. Solloway[1], Bernard B. Allan[1], Avantika Kekatpure[1], Shelley R. Starck[1], Raj Haldankar[1], Bin Fan[1], Chun Chu[1], Jie Tang[1], Martina Molgora[2], Marco Colonna[2], Daniel D. Kaplan[1], and Jer-Yuan Hsu[1]

ABSTRACT

Suppressive myeloid cells inhibit antitumor immunity by preventing T-cell responses. Immunoglobulin-like transcript 3 (ILT3; also known as LILRB4) is highly expressed on tumor-associated myeloid cells and promotes their suppressive phenotype. However, the ligand that engages ILT3 within the tumor microenvironment and renders tumor-associated myeloid cells suppressive is unknown. Using a screening approach, we identified fibronectin as a functional ligand for ILT3. The interaction of fibronectin with ILT3 polarized myeloid cells toward a suppressive state, and these effects were reversed with an ILT3-specific antibody that blocked the interaction of ILT3 with fibronectin. Furthermore, *ex vivo* treatment of human tumor explants with anti-ILT3 reprogrammed tumor-associated myeloid cells toward a stimulatory phenotype. Thus, the ILT3–fibronectin interaction represents a "stromal checkpoint" through which the extracellular matrix actively suppresses myeloid cells. By blocking this interaction, tumor-associated myeloid cells may acquire a stimulatory phenotype, potentially resulting in increased antitumor T-cell responses.

Introduction

The success of immune checkpoint inhibitors in cancer therapy depends on the ability of effector T cells to infiltrate the tumor and mediate cytotoxicity against cancer cells. Despite the clinical success of checkpoint blockade therapies, tumors employ multiple mechanisms to subvert the desired antitumor response. Although the mechanisms of resistance are not fully understood, a high stromal content is a major contributor to both T-cell exclusion and resistance to immune checkpoint blockade in human patients with cancer (1–4).

A major constituent of the tumor stroma is the extracellular matrix (ECM), which is gaining increasing recognition as a cause of immunosuppression within the tumor microenvironment (TME). For example, degradation of collagen increases T-cell penetration of human tumor explants, enabling direct contact between T cells and tumor cells (5). In a mouse tumor model, depletion of fibroblasts by vaccination against fibroblast-activating protein (FAP) decreases collagen deposition and improves responses to immune checkpoint blockade (6). Although these effects have generally been attributed to the ECM acting as a physical barrier to immune-cell entry, emerging evidence suggests that ECM components can directly alter the functional properties of immune cells in the TME. For example, the collagen receptor leukocyte-associated immunoglobulin-like receptor 1 (LAIR1) was recently linked to $CD8^+$ T-cell exhaustion and immunotherapy resistance in human patients with cancer (7). In addition, in mouse studies, significant tumor regression is only achieved when immune checkpoint inhibitors are combined with agents targeting stromal-mediated mechanisms of immunosuppression (LAIR1 or TGFβ; refs. 7, 8). However, the mechanisms through which the ECM modulates immune cells, particularly myeloid cells, are only beginning to be elucidated. Understanding how the ECM communicates with myeloid cells will be fundamental in uncovering mechanisms of ECM-based immunosuppression, potentially defining a new class of "stromal checkpoint" molecules for cancer immunotherapy.

Dendritic cells (DC) regulate the balance between tolerance and immunity in many tissues, including tumors. Within the TME, DCs acquire tumor-associated antigens released by dying cells in the hypoxic tumor core (9). Once activated, mature DCs migrate to the draining lymph node, where they prime naïve T cells. Interactions between mature DCs and naïve antigen-specific T cells promote T-cell clonal expansion and the acquisition of T-cell effector function, resulting in T cell–mediated antitumor immunity. However, DCs that have been exposed to immunosuppressive factors such as TGFβ acquire a tolerogenic phenotype characterized by reduced expression of costimulatory molecules, impaired antigen uptake and presentation, and decreased production of proinflammatory cytokines. Interactions between naïve T cells and such tolerogenic DCs result in suboptimal T-cell activation, anergy, or differentiation into regulatory T cells (10, 11). These immunosuppressive factors are expressed in healthy

[1]NGM Biopharmaceuticals, South San Francisco, California. [2]Department of Pathology and Immunology, Washington University School of Medicine, St. Louis, Missouri.

Note: Supplementary data for this article are available at Cancer Immunology Research Online (http://cancerimmunolres.aacrjournals.org/).

K.J. Paavola and J.M. Roda contributed equally to this article.

Current address for G. Horner: Just Biotherapeutics, Seattle, Washington; current address for Z. Zhang, Ambagon Therapeutics Inc., San Francisco, California; and current address for B.B. Allan, Takeda Pharmaceuticals International Co., Cambridge, Massachusetts.

Corresponding Author: Jer-Yuan Hsu, NGM Biopharmaceuticals, 333 Oyster Point Boulevard, South San Francisco, CA 94080. Phone: 650-243-5579; Fax: 650-583-1646; E-mail: ahsu@ngmbio.com

Cancer Immunol Res 2021;9:1283–97

doi: 10.1158/2326-6066.CIR-21-0240

tissues to promote peripheral tolerance, but their production by tumor cells prevents antitumor immunity (12). The presence of tolerogenic DCs within the TME correlates with poor prognosis in a number of cancer types (13–15).

Immunoglobulin-like transcript 3 (ILT3) is a cell surface receptor of the immunoglobulin (Ig) superfamily that is expressed on myeloid cells and transmits intracellular inhibitory signals through cytoplasmic immunoreceptor tyrosine-based inhibitory motifs (ITIM; ref. 16). ILT3 is highly expressed by tolerogenic DCs derived *in vitro* (17). Although ILT3 is upregulated in response to numerous tolerizing factors (10, 18), and an antibody against ILT3 can impede the inhibition of T cells by tolerogenic DCs (17), the specific mechanisms through which ILT3 on tolerogenic DCs promotes antigen-specific immune tolerance are poorly understood. Although several biochemical ligands for ILT3 have been reported, functional effects of these receptor–ligand interactions on primary immune cells have not been demonstrated (19–21). Here, we show that the ECM protein fibronectin is a functional ligand for ILT3. The interaction of fibronectin with ILT3 polarized myeloid cells toward a suppressive state, decreasing their production of T cell–recruiting chemokines, and eliminating their ability to stimulate T-cell proliferation. Furthermore, fibronectin treatment rendered DCs unresponsive to stimulation via Fcγ receptor (FcR) ligation. These effects were reversed with an ILT3-specific antibody that blocked the ILT3–fibronectin interaction. The engagement of ILT3 by fibronectin thus represents a stromal checkpoint through which the ECM can signal via an inhibitory immune receptor to directly promote myeloid cell suppression within the TME.

Materials and Methods

Antibodies and reagents

The following primary antibodies were used: rabbit anti-human SYK, clone 2712 (Cell Signaling Technology, catalog no. 2712, RRID: AB_2197223, 1:1,000 dilution); rabbit anti-human SHP1, clone C14H6 (Cell Signaling Technology, catalog no. 3759, RRID: AB_2173694, 1:1,000 dilution); rabbit anti-human SHP2, clone D50F2 (Cell Signaling Technology, catalog no. 3397, RRID: AB_2174959, 1:1,000 dilution); rabbit anti-human GAPDH, clone D16H11 (Cell Signaling Technology, catalog no. 5174, RRID: AB_10622025, 1:1,000 dilution); and rabbit anti-fibronectin, clone F14 (Abcam, catalog no. ab45688, RRID: AB_732380, 1:1,000 dilution). For immunofluorescence studies, the IRDye 800CW anti-rabbit (LI-COR Biosciences, catalog no. 926-32211, RRID: AB_621843) and IRDye 800CW anti-mouse (LI-COR Biosciences, catalog no. 926-32210, RRID: AB_621842) were used at 1:10,000 dilutions. PE-labeled anti-human ILT3, clone ZM4.1 (BioLegend, catalog no. 333008, RRID: AB_2136645) was used for flow cytometric analysis of ILT3 expression.

Cell lines

The source and culture conditions for the 110 cell lines used in the ILT3-GFP reporter cell screen are detailed in Supplementary Table S1. The human epithelial HEK293T (catalog no. CRL-3216, RRID: CVCL_0063, obtained in 2011 to 2012), mouse myeloma SP2/0 (catalog no. CRL-1581, RRID: CVCL_2199, obtained in 2012 to 2013), retroviral packaging Phoenix-AMPHO (catalog no. CRL-3213, RRID: CVCL_H716, obtained in 2014), and human leukemia THP-1 (catalog no. TIB-202, RRID: CVCL_0006, obtained in 2012 to 2013) cell lines were all obtained from the ATCC. HEK293T and Phoenix-AMPHO cells were maintained in DMEM (Corning, catalog no. 10-013-CM) supplemented with 10% FBS (Gibco, catalog no. 16000-044) and 1% penicillin/streptomycin (Corning, catalog no. 30-002-CL). SP2/0 and THP-1 cells were maintained in RPMI1640 (Corning, catalog no. 10-040-CM) supplemented with 10% FBS and 1% penicillin/streptomycin. The human stellate cell line LX-2 (catalog no. SCC064, RRID: CVCL_5792) was obtained from Sigma-Aldrich in 2016. The human epithelial Expi293 cell line (catalog no. A14527, RRID: CVCL_D615) was purchased from Thermo Fisher Scientific in 2015. Expi293 cells were maintained in Expi293 Expression Medium (Thermo Fisher Scientific, catalog no. A1435101). The CT237 reporter cell line, which stably expresses DAP12 and a NFAT-driven GFP reporter (22), was maintained in RPMI1640 supplemented with 10% FBS and 1% penicillin/streptomycin. To generate the ILT3-GFP reporter cells, cDNA encoding the human ILT3 extracellular domain (ECD; M1-E259) fused to the transmembrane and intracellular domains of human PILRB (V192-F227) was cloned into the pBABE-puro vector (CellLabs, catalog no. RTV-001-PURO) and transfected into the retroviral packaging cell line Phoenix-AMPHO with Lipofectamine 2000 (Thermo Fisher Scientific, catalog no. 11668019) to generate retroviral particles. CT237 cells were transduced with the retroviral particles by centrifugation at 1,300 rpm for 2 hours in the presence of 8 μg/mL polybrene infection reagent (Sigma-Aldrich, catalog no. TR-1003). All cell lines were expanded and frozen stocks made after 2 to 3 passages. No more than 10 passages for HEK293T, THP-1, Phoenix-AMPHO, and LX-2 cells and no more than 20 passages for Expi293 cells were used before new stocks were thawed for experimental use. SP2/0 cells were thawed and passaged twice before using for electrofusion with B cells from immunized animals. There was no further authentication or *Mycoplasma* testing performed on any purchased cell lines after provided manufacturer validation.

Analyses of *ILT3* expression using data from The Cancer Genome Atlas and The Genotype Tissue Expression Project

To determine expression levels of *ILT3* in human tumors versus normal tissues, RNA-sequencing (RNA-seq) data were acquired from 9,889 tumor samples spanning 33 cancer indications from The Cancer Genome Atlas (TCGA) and 9,052 normal tissue samples spanning 30 tissues from The Genotype-Tissue Expression (GTEx) project. Data were extracted from QIAGEN OmicSoft OncoLand (releases GTEx_B38_GC33_20210701_v2 and TCGA_B38_GC33_20210315_v1). OncoLand data, although from two sources, were made comparable by alignment to human genome B38 with OmicsoftGenCode.V33, using OSA (23), and were quantified using RSEM (24).

Generation of ECD-Fc fusion proteins

The Fc-tagged ILT3 ECD (ILT3-Fc) expression plasmid was constructed in a pTT5 vector (NovoPro, catalog no. V001466) with the following elements from N- to C-termini: a signal peptide (human Igκ), ILT3 ECD (G24-E259 of natural variant G223), a flexible linker (three repeats of GGGGS), and human IgG1 Fc (IMGT allele IGHG1*3). The LAIR1-Fc expression plasmid utilized the same pTT5 vector, signal peptide, and human IgG1 Fc as above and contained LAIR1 ECD (Q22-Y165 of natural variant D63) and two glycine residues as a linker. The human Fc-only control expression plasmid contained only the signal peptide and human IgG1 Fc. To express the proteins, plasmid DNA was transfected into Expi293 cells using the ExpiFectamine Transfection kit (Thermo Fisher Scientific, catalog no. A14525). After 5 to 6 days incubation, conditioned media were harvested and the proteins were purified at room temperature using a fast protein liquid chromatography (FPLC) system (GE Healthcare/Cytiva). Media was applied to 5 mL HiTrap MabSelect SuRe (Cytiva,

catalog no. 11003494) resin at 5 mL/minute. The resin was washed with PBS (Thermo Fisher Scientific, catalog no. BP3991) and eluted with 0.5% acetic acid adjusted to pH 3.5. Protein-containing fractions were neutralized with 1/10th volume of 1 mol/L Tris, pH 8.0 (Teknova, catalog no. T1080), and concentrated to 5 mL by ultrafiltration (Millipore, catalog no. UFC903008, 30 kDa MWCO). Proteins were then subjected to size-exclusion chromatography by injecting into a Superdex 200 26/600 (Cytiva, catalog no. 28989336) equilibrated with 25 mmol/L HEPES, 150 mmol/L NaCl, pH 7.5 at a flow rate of 2.5 mL/minute. Protein-containing fractions from the major peak corresponding to approximately 100 kDa (fusion proteins) or 50 kDa (Fc control) were pooled and concentrated. Protein identities were confirmed by mass spectrometry (MS; Agilent 6520 Accurate Mass QTOF, Model G6520B) and purities were determined to be >98% monodispersed on a size exclusion column (Yarra SEC-3000, Phenomenex) using a high-performance liquid chromatography (HPLC; Series 1200, Agilent).

Generation of anti-ILT3 antibody 16C5

B6.129 mice, age 7 to 8 weeks (The Jackson Laboratory, strain 101043), were immunized twice weekly with the His-tagged ECD of human ILT3 protein (R&D Systems, catalog no. 8488-T4). All animal experiments were conducted in accordance with, and with the approval of, the NGM Institutional Animal Care Use Committee (IACUC). After nine injections, lymph nodes and spleens were harvested from the animals, dissociated into single-cell suspensions, and fused with SP2/0 myeloma cells using the ECFG21 Super Electro Cell Fusion Generator (Nepagene) to generate hybridomas. Hybridomas were plated in a semi-solid media (ClonaCell Medium D, StemCell Technologies, catalog no. 03834), and single-cell colonies were picked using Clonepix (Molecular Devices). To screen for ILT3 binders, 25 μL of conditioned media from each hybridoma were incubated for 30 minutes at room temperature with Expi293 cells transiently transfected with a pCMV6-XL5 expression plasmid encoding full-length ILT3 (Origene, catalog no. SC115840) using Lipofectamine 2000 (Thermo Fisher Scientific, catalog no. 11668500). Cells were then washed and incubated with an APC-labeled goat anti-mouse (Jackson ImmunoResearch, catalog no. 115-606-071). Data were acquired on a FACSCalibur flow cytometer (BD Biosciences) and analyzed using FlowJo software, version 10.0 (BD Biosciences). The specific binding of anti-ILT3 clone 16C5 was confirmed by flow cytometry as described above, using Expi293 cells transfected with expression constructs encoding human ILT family members [LILRA1: SINOHG17220-CF (Sino Biologicals), LILRA2: RC205626, LILRA4: RC220452, LILRA5: RC212310, LILRA6: RC212965, LILRB1: SC320409, LILRB2: SC321856, LILRB3: SC108531, LILRB4: SC115840, and LILRB5: SC322552 (Origene)].

The variable regions of heavy chain and light chain of 16C5 were determined by DNA sequencing following RT-PCR as described previously (25) and cloned into the pTT5 vector (NovoPro, catalog no. V001466). The plasmids encoding the light and heavy chains were cotransfected into Expi293 cells using the ExpiFectamine Transfection kit (Thermo Fisher Scientific, catalog no. A14525). After 5 to 6 days incubation, conditioned media was clarified by centrifugation and sterile filtration. Antibodies were purified at room temperature using an FPLC system (GE/Cytiva) executing an automated three-step purification method at a flow rate of 5 mL/minute. Media was applied to 5 mL HiTrap MabSelect SuRe (Cytiva, catalog no. 11003494) resin. The resin was washed with PBS (Thermo Fisher Scientific, catalog no. BP3991) and eluted with 0.5% acetic acid adjusted to pH 3.5. The antibodies were then injected into a HiPrep 26/10 desalting column (Cytiva, catalog no. 17508701) equilibrated in a solution of 25 mmol/L sodium acetate, pH 5.5. The peak of antibodies was then injected into a 5 mL HiTrap SP HP column (Cytiva, catalog no. 17115201) equilibrated with 25 mmol/L sodium acetate, pH 5.5. Antibodies were eluted and fractionated using a 100 mL (20 column volume) linear gradient from 0 to 500 mmol/L NaCl buffered with 25 mmol/L sodium acetate, pH 5.5. Aggregate-free IgG-containing fractions determined by SDS-PAGE analysis were pooled and formulated by two rounds of concentration (Millipore, catalog no. UFC903008, 30 kDa MWCO) and 10-fold dilution with 25 mmol/L HEPES, 150 mmol/L NaCl, and pH 7.4. Antibody chain identities were confirmed by MS (Agilent, 6520 Accurate Mass QTOF, Model G6520B), and purities determined to be >98% monodispersed on a size exclusion column (Phenomenex, Yarra SEC-3000) using an HPLC (Agilent, Series 1200), and endotoxin levels measured to be < 1 EU/mg protein (Charles River, catalog no. PTS201F).

Cell line screen for putative ILT3 ligand

The CT273-based ILT3-GFP reporter cells were cocultured with each of the 110 cell lines (Supplementary Table S1) and the activation of GFP was detected by flow cytometry. Briefly, the ILT3-GFP reporter cells were first labeled with CellTracker Deep Red dye at a 1:4,000 dilution (Thermo Fisher Scientific, catalog no. C34565) for 30 minutes at 37°C in PBS. The labeled ILT3-GFP reporter cells and the test cell lines were then equilibrated with RPMI1640 containing 10% FBS and then mixed at a 1 to 4 ratio (1×10^5 reporter cells to 4×10^5 test cell line) and incubated overnight at 37°C in triplicate wells of a 96-well tissue culture plate. The labeled ILT3-GFP reporter cells were assayed for GFP expression by flow cytometry and compared with unstimulated reporter cells.

Immunoprecipitation of LX-2 cells and MS

LX-2 cells were plated at 2.5×10^6 cells in a 150 mm tissue culture dish and incubated for 3 days in DMEM containing 10% FBS, 1% penicillin-streptomycin, and (for activated LX-2 cells) 2.5 ng/mL TGFβ (Peprotech, catalog no. 100-21). Media was aspirated and the cells were lysed in 100 μL of cell lysis buffer (Cell Signaling Technology, catalog no. 9803) comprised of 20 mmol/L Tris-HCl (pH 7.5), 150 mmol/L NaCl, 1 mmol/L Na_2EDTA, 1 mmol/L EGTA, 1% Triton, 2.5 mmol/L sodium pyrophosphate, 1 mmol/L β-glycerophosphate, 1 mmol/L Na_3VO_4, 1 μg/mL leupeptin and supplemented with HALT phosphatase/protease inhibitor cocktail (Thermo Fisher Scientific, catalog no. 78444). Lysates were cleared by spinning at >16,000 rcf at 4°C for 10 minutes, and cleared lysates were quantified by Pierce bicinchoninic acid assay (Thermo Fisher Scientific, catalog no. 23225). Immunoprecipitation was performed using Invitrogen Protein G Dynabeads (Thermo Fisher Scientific, catalog no. 10004D) according to the manufacturer's instructions. Briefly, 10 μg of ILT3-Fc or control human Fc (generated as described in "Generation of ECD-Fc fusion proteins") was bound to 50 μL of magnetic Dynabeads for 30 minutes at 4°C. Supernatant was removed and protein lysate was added. For each treatment condition, lysate containing approximately 615 μg of total protein was added to the Dynabead complex and incubated overnight at 4°C with gentle rotation. Protein lysates were removed, and Dynabeads were washed three times with 200 μL of lysis buffer for 5 minutes per wash. Protein was eluted from the Dynabeads with 50 μL of elution buffer, comprised of protein loading buffer (LI-COR Biosciences, catalog no. 928-40004) containing 125 mmol/L Tris-HCl (pH 6.8), 50% glycerol, 4% SDS, and 0.2% (w/v) Orange G, Invitrogen NuPAGE sample reducing agent (Thermo Fisher Scientific, catalog no. NP0009) containing 500 mmol/L dithiothreitol, and lysis buffer (Cell Signaling Technology, catalog no. 9803) in a

ratio of 15:4:1. The proteins were eluted at 95°C for 5 minutes. To identify bands of interest, silver stain analysis was performed on 10 μL of the protein eluate using the PlusOne kit (GE Healthcare, catalog no. 17-1150-01) according to the manufacturer's instructions. Silver-stained gels were imaged using the Gel Doc EZ system (Bio-Rad).

For MS analysis, gel electrophoresis was performed on the remaining 40 μL of eluate and processed as described below. The gel was stained with Bio-Safe Coomassie Stain (Bio-Rad, catalog no. 161-0787). Gel bands were excised in a biological safety cabinet and sliced into small fragments. Gel pieces were washed in 50% acetonitrile and 200 mmol/L ammonium bicarbonate, then incubated in 100% acetonitrile for 10 minutes and dried in a SpeedVac vacuum concentrator. Proteins in the gel pieces were then reduced and alkylated by sequential incubation with 25 mmol/L tris(2-carboxyethyl)phosphine and 50 mmol/L iodoacetamide. Gel pieces were washed and incubated with acetonitrile again, then digested with trypsin (Promega, catalog no. V507A) at 20 μg/mL in 50 mmol/L ammonium bicarbonate, pH 8.0 overnight at 37°C.

Digested samples were then analyzed by MS. Briefly, peptides were separated over an EASY-Spray PepMap C18 column (Thermo Fisher Scientific, catalog no. ES900) connected to an Ultimate RSLC nanoLC system (Thermo Fisher Scientific, catalog no. ULTIM3000RSLC-NANO). Peptides were eluted from the column by ramping from 2% to 32% acetonitrile over 135 minutes and injected into an Orbitrap Velos Pro mass spectrometer. LC/MS-MS data were collected using a top10 method, with MS data collected at 60,000 resolution from 200 to 2,000 m/z. MS-MS data were collected with dynamic exclusion, monoisotopic precursor selection, and charge state screening enabled on the ion trap. Singly charged peptides were excluded. Raw files were analyzed with PEAKS X proteomics software (Bioinformatics Solutions) searching against a database of human proteins. In PEAKS, proteins were identified with a −10logp setting of 20 and an FDR of no higher than 1.5%. Hits were ranked by total peptide count, and extracellular or transmembrane proteins that were found in experimental samples but not controls were identified.

CRISPR/Cas9-mediated knockout of human fibronectin in LX-2 cells

To generate fibronectin knockout LX-2 cells, three guide RNAs (gRNA) targeting individual gene sequences of *FN1*, identified here by the manufacturer provided CRISPR gRNA ID numbers, were purchased from IDT (CRISPR gRNA ID; sequence: Hs.Cas9.FN1.1.AA; GACCTACCTAGGCAATGCGT, Hs.Cas9.FN1.1.AB; CTATGTGG-TCGGAGAAACGT, and Hs.Cas9.FN1.1.AC; ACTGGGAACACT-TACCGAGT). All three gRNAs were mixed with Alt-R S.p. Cas9 Nuclease V3 (IDT, catalog no. 1081059) to form Cas9-gRNA ribonucleoprotein (6 μL gRNA at 20 μmol/L mixed with 2 μL of Cas9 at 61 μmol/L). The Cas9-gRNA mixture was incubated at room temperature for 20 minutes to form the ribonucleoprotein complex. To electroporate LX-2 cells with Cas9-gRNA ribonucleoprotein, 2×10^5 LX-2 cells were resuspended in 17.5 μL of SF buffer (Lonza, catalog no. V4XC-2032), combined with 2.5 μL of ribonucleoprotein, and electroporated with program CA-137 of a Lonza Nucleofector.

Immunocytochemistry of LX-2 cells

LX-2 cells were cultured for 3 days in the presence or absence of TGFβ (Peprotech, catalog no. 100-21). Human ILT3ECD-Fc (5 μg/mL) was added for 30 minutes at room temperature, and the cells were fixed with 4% paraformaldehyde for 10 minutes. In some experiments, Fc-tagged human B7-H4 ECD (B7-H4-Fc; R&D Systems, catalog no. 8870-B7) was used as a negative control for LX-2 cell binding. Cells were blocked (10% FBS, 1% BSA, 0.01% NaN_3 in PBS) at room temperature for 1 hour, then incubated with rabbit anti-fibronectin clone F14, which is cross-reactive to human and mouse fibronectin (Abcam, catalog no.: ab45688, RRID: AB_732380), at a 1:500 dilution for 1 hour at room temperature. Cells were then washed and stained with secondary antibodies, either AlexaFluor 488–conjugated anti-rabbit (Jackson ImmunoResearch, catalog no. 111-546-046, RRID: AB_2338055, 1:1,000 dilution) or AlexaFluor 647–conjugated anti-human (Jackson ImmunoResearch, catalog no. 109-606-098, RRID: AB_2337899, 1:500 dilution), for 1 hour at room temperature. Nuclei were stained with Hoechst (Thermo Fisher Scientific, catalog no. PI62249, 1:10,000 dilution) for 10 minutes at room temperature. Cells were imaged using a Nikon Ti2-E inverted microscope equipped with a 20 × 0.75 NA Plan Apo objective (Nikon), a DS-Qi2 monochrome CMOS camera (Nikon) and a Sola SE II 360 Light Engine (Lumencor).

Evaluation of ILT3–fibronectin biochemical binding by surface plasmon resonance

Human plasma fibronectin (Millipore, catalog no. FC010) and collagen type IV (Millipore, catalog no. CC076) were first immobilized onto CM5 sensor chip surfaces using amine coupling chemistry. Briefly, equal volumes of 0.48 mol/L 1-ethyl-3-(3-demethylaminopropyl)carbodiimide hydrocyloride (Thermo Fisher Scientific, catalog no. 22980) and 0.1 mol/L N-hydroxylsulfosuccinimide (Thermo Fisher Scientific, catalog no. 24510) were mixed and injected for 7 minutes to activate the CM5 chip surface. This was followed by injection of fibronectin or collagen on two different flow cells at 50 μg/mL in acetate buffer (pH 4.0) for 7 minutes. A reference surface was treated as above without the proteins. From a starting concentration of 50 μg/mL of each protein, it was determined that 14,111 response units of fibronectin and 2,891 response units of collagen were immobilized onto the respective chips. Human ILT3-Fc or human LAIR1-Fc (generated as described in "Generation of ECD-Fc fusion proteins") were injected over both surfaces at different concentrations (125–4,000 nmol/L) to evaluate binding kinetics and affinity at 25°C using the Biacore T200 system.

Activation of ILT3 reporter cells by fibronectin or ApoE

First, 96-well Maxisorp (Nunc) plates were coated with 5 μg/mL of human Fc protein (R&D Systems, catalog no. 110-HG), human collagen type I (Millipore, catalog no. CC050), human laminin (R&D Systems, catalog no.: 7340-A4), plasma-derived human fibronectin (Millipore, catalog no. FC010), recombinant human fibronectin (R&D Systems, catalog no.: 4305-FNB), or recombinant human ApoE2 (Peprotech, catalog no. 350-12) in PBS at room temperature for 2 hours. Plates were washed twice with PBS and blocked with RPMI1640 containing 10% FBS, then ILT3 NFAT-GFP reporter cells were added to the coated wells (1×10^5 cells/well) and incubated overnight at 37°C. In some experiments, an isotype control antibody or an in-house anti-ILT3 antibody (clone 16C5, generated as described in "Generation of anti-ILT3 antibody 16C5") was added to the wells at a final concentration of 5 μg/mL. Cells were assayed for GFP expression by flow cytometry and compared with unstimulated reporter cells.

Generation of ILT3 knockout THP-1 cells and THP-1 cells with tyrosine-modified ILT3

The human leukemic monocyte cell line THP-1 was cultured in RPMI1640 containing 10% FBS and 1% penicillin/streptomycin. ILT3

knockout THP-1 cells were generated using CRISPR/Cas9-based gene editing using TrueCut Cas9 Protein v2 (Thermo Fisher Scientific, catalog no. A36499) complexed with Invitrogen TrueGuide sgRNA Modified gRNA targeting two individual sequences of *LILRB4* (CRISPR gRNA ID; sequence: CRISPR1072704_SGM; GGAACAACCCCATGACGAGA and CRISPR1072708_SGM; AGCCGTGAAGGTGGGGATCA, Thermo Fisher Scientific, catalog no. A35533). To generate THP-1 cells carrying ILT3 with ITIM mutations (Y359F, Y411F, and Y441F), plasmid DNA containing the ITIM mutations was first generated using the Site-Directed Mutagenesis System (Thermo Fisher Scientific, catalog no. A13282) and then submitted to G&P Biosciences for retroviral particle production. ILT3 knockout THP-1 cells were then transduced with the retroviral particles using the RetroNectin system (Takara, catalog no. T100A). Briefly, tissue culture plates were precoated with RetroNectin protein, then viral particles were added and the plates were centrifuged at 1,000 $\times$ *g* for 2 hours at 32°C. ILT3 knockout THP-1 cells were then added and incubated for 3 days at 37°C. Transduced cells were sorted on ILT3 expression using the APC-labeled anti-human ILT3, clone ZM4.1 (Thermo Fisher Scientific, catalog no. 17-5139-42) on an Aria II cell sorter (BD Biosciences). Bulk pools of cells were expanded and the ILT3 expression status on the cell surface was verified by flow cytometry.

Suppression of FcR-driven cytokine production by fibronectin or ApoE

Wells of a 96-well Maxisorp (Nunc) plate were co-coated with fibronectin (Millipore, catalog no. FC010) or ApoE2 (Peprotech, catalog no. 350-12) with human anti-KLH (each at 5 μg/mL in PBS) at room temperature for 2 hours, then washed twice with PBS and preincubated with RPMI1640 containing 10% FBS for 2 hours. THP-1 cells (2×10^5 cells/well) or tolerogenic human DCs (7×10^4 cells/well; generated as described in "Differentiation of primary human DCs and generation of knockout DCs") were plated on the coated wells. In some experiments, cells were washed, resuspended in X-Vivo 15 media (Lonza, catalog no. 04-418Q), and incubated with the designated antibodies (5 μg/mL) in solution at room temperature for 20 minutes before plating onto coated wells. After overnight incubation at 37°C, culture supernatants were collected, and cytokine secretion was measured by Luminex assay using human IL8 simplex kits (Thermo Fisher Scientific, catalog no. EPX01A-10204-901, RRID: AB_2575769) or human TNFα simplex kits (Thermo Fisher Scientific, catalog no. EPX01A-10223-901, RRID: AB_2575781) according to the manufacturer's instructions.

Differentiation of primary human DCs and generation of knockout DCs

Human peripheral blood mononuclear cells (PBMC) of healthy donors were isolated from freshly drawn leukopaks (Allcells, catalog no. PB007) by density gradient centrifugation over Ficoll Histopaque Plus (GE Healthcare, catalog no. 17-1440-03) and frozen in CryoSTOR CS10 cell preservation medium (StemCell Technologies, catalog no. 07930) for future use. Primary human monocytes were isolated from freshly thawed PBMCs by negative selection using the Miltenyi Human Monocyte Isolation Kit (Miltenyi Biotec, catalog no. 130-096-537) and plated at 2×10^6 cells/mL in X-Vivo 15 media (Lonza, catalog no. 04-418Q). Monocytes were treated with 50 ng/mL of recombinant human GM-CSF (Peprotech, catalog no. 300-03) and IL4 (Peprotech, catalog no. 200-04) for 5 days to generate monocyte-derived DCs (moDC), then tolerized by the addition of 10 nmol/L dexamethasone (Sigma, catalog no. D4902) and 100 nmol/L vitamin D3 (1α,25-dihydroxyvitamin D3; Sigma, catalog no. D1530) for 2 days. Tolerogenic DCs had increased expression of ILT3, had poor allostimulatory capacity, and were able to actively suppress T-cell activation induced by allogeneic moDCs, as described previously (18).

To generate knockout DCs, three gRNAs targeting individual gene sequences were purchased from Thermo Fisher Scientific (catalog no. A35533). Manufacturer-provided CRISPR gRNA ID numbers; sequences for each gene are as follows. ILT3: CRISPR1072704_SGM; GGAACAACCCCATGACGAGA, CRISPR808548_SGM; GCATAGTCCTCTGTCATGGA, and CRISPR808534_SGM; CAGGGCTGCGATAGTAACAG; SHP1: CRISPR797887_SGM; GGTTTCACCGAGACCTCAGT, CRISPR797888_SGM; GGGATCAGGTGACCCATATT, and CRISPR797910_SGM; GAGTACTACACTCAGCAGCA; SHP2: CRISPR707279_SGM; GGTTTCATGGACATCTCTCT, CRISPR707293_SGM; ACGGAAAGTGTGAAGTCTCC, and CRISPR707312_SGM; CGTGATGTTCCATGTAATAC; SYK: CRISPR819114_SGM; TTTCGGCAACATCACCCGGG, CRISPR819133_SGM; GCAGAAGATTACCTGGTCCA, and CRISPR819123_SGM; CACACCACTACACCATCGAG. All three gRNAs for a given gene were mixed with Alt-R S.p. Cas9 Nuclease V3 (IDT, catalog no. 1081059) to form Cas9-gRNA ribonucleoprotein (7 μL gRNA at 50 μmol/L mixed with 3.5 μL of Cas9 at 61 μmol/L). The Cas9-gRNA mixture was incubated at room temperature for 20 minutes for ribonucleoprotein complex formation. To nucleofect primary human monocytes with Cas9-gRNA, 5×10^6 cells were resuspended in 100 μL of P3 working buffer (Lonza, catalog no. V4XP-3024), combined with 5 μL of ribonucleoprotein, and nucleofected using the 4D nucleofector system (Lonza) with the human primary monocyte program. Monocytes were then differentiated into DCs as described above.

RNA-seq of myeloid cell populations treated with fibronectin and/or anti-ILT3

Tissue culture–treated plates were precoated with PBS or 5 μg/mL of fibronectin (Millipore, catalog no. FC010) overnight at 4°C, then washed with PBS and preincubated with X-Vivo 15 media (Lonza, catalog no. 04-418Q) for 30 minutes. Primary human monocytes were added to coated wells in the presence of 5 μg/mL of anti-KLH (negative control antibody) or anti-ILT3 (clone 16C5) and differentiated into moDCs or tolerogenic DCs as described above ("Differentiation of primary human DCs and generation of knockout DCs"). After 7 days, supernatants were collected for analysis of circulating chemokines by Luminex assay using the human CCL3 (Thermo Fisher Scientific, catalog no. EPX01A-12029-901, RRID: AB_2575832) and human CCL4 (Thermo Fisher Scientific, catalog no. EPX01A-12030-901, RRID: AB_2575833) simplex kits according to the manufacturer's instructions. For collection of RNA, cells were lysed in Invitrogen TRIzol reagent (Thermo Fisher Scientific, catalog no. 15596018). Total RNA was isolated from TRIzol by extraction with chloroform and purified using the RNeasy Mini Kit (Qiagen, catalog no. 74004). RNA concentrations were determined using a NanoDrop spectrophotometer, and sample quality was confirmed by Bioanlyzer (Agilent). All samples had RNA integrity numbers ≥ 9.7. Total RNA was prepared for sequencing using the TailorMix Directional RNA Sample Preparation Kit (SeqMatic, catalog no. TM200-A) and sequenced on an Illumina NovaSeq S1 (100 bp single-end reads; an average of 24 million reads were generated for each sample). For sequencing alignment, the raw reads were filtered using Trim Galore! (http://www.bioinformatics.babraham.ac.uk/projects/trim_galore/) to remove low-quality and adaptor bases, and reads shorter than 20 nt were discarded. Filtered reads were mapped to UCSC hg19 genome sequences using STAR (v2.6.0a). Finally, counts of all samples were generated using

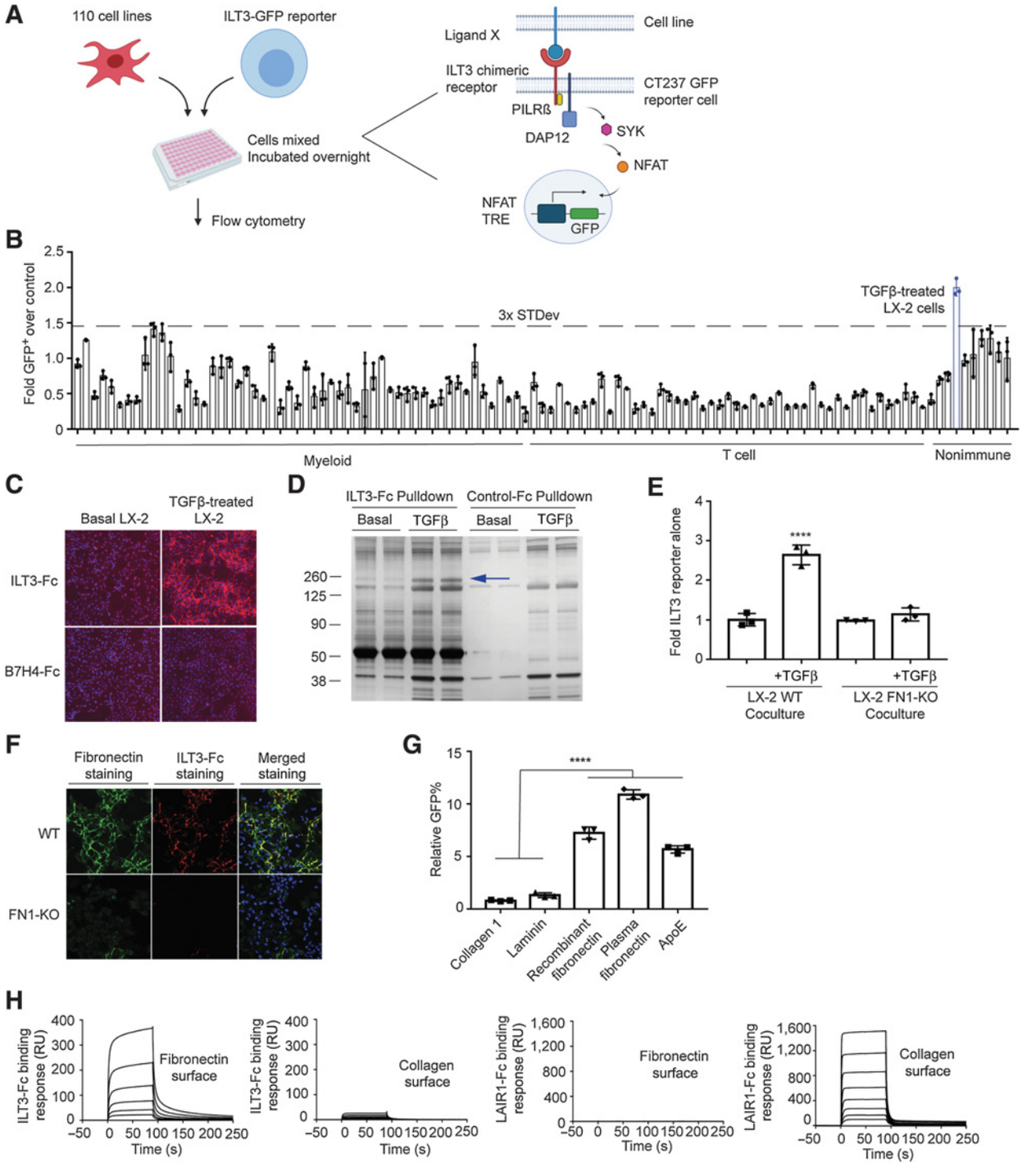

Figure 1.

Fibronectin is a binding partner of ILT3. **A,** Schematic representation of the cell line screen using ILT3 reporter cells. A collection of 110 cell lines were cocultured overnight with a reporter cell line (CT237 GFP) expressing the ILT3 ECD fused to the transmembrane domain of PILRβ, which pairs with DAP12. Upon ligand binding to ILT3, the ITAM of DAP12 activates the SYK/NFAT signaling cascade, resulting in GFP gene expression driven by the NFAT transcriptional response element (TRE). **B,** The results of the cell line screen using the ILT3 reporter cells. A collection of 110 cell lines representing myeloid cells, T cells, and nonimmune cell types were screened. Results are expressed as the fold change in GFP^+ reporter cells relative to reporter cells cultured alone. A positive hit was arbitrarily defined as the fold GFP^+ change that is >3 standard deviations (STDev) from the mean of all cell lines tested ($n = 1$, with three technical replicates). **C,** Basal (left) or TGFβ-treated (right) LX-2 cells were immunofluorescence stained with ILT3-Fc (top) or B7-H4-Fc (bottom) with 10× magnification (independent experiment ≥ 3). **D,** Representative SDS-PAGE analysis of affinity-purified LX-2 cell lysates. (*Continued on the following page.*)

featureCounts (v1.6.2), and edgeR (v3.22.3; refs. 26, 27) was used to obtain normalized counts and perform differential gene expression analysis. The data have been deposited into the Gene Expression Omnibus as GSE175354.

Allogeneic mixed lymphocyte reactions with LX-2 cells

Tolerogenic DCs were generated as described above ("Differentiation of primary human DCs and generation of knockout DCs") and resuspended to a density of 4×10^5 cells/mL. TGFβ-treated (2.5 ng/mL, overnight) wild-type or fibronectin knockout LX-2 cells were treated with 25 μg/mL mitomycin C (Sigma-Aldrich, catalog no. M7949) to inhibit cell proliferation for 1 hour at 37°C, washed, and resuspended to a density of 1×10^5 cells/mL. Allogeneic T cells were purified from PBMCs by negative selection using the Miltenyi human pan T Cell Isolation Kit (Miltenyi Biotec, catalog no. 130-096-535) and resuspended to a density of 2×10^6 cells/mL. Wells of a 96-well, round-bottom plate were prefilled with 50 μL of anti-KLH or anti-ILT3 antibody at 20 μg/mL. Mixed lymphocyte reactions were established by adding 50 μL of each cell type at the densities indicated above, for a final T cell:DC:LX-2 cell ratio of 20:2:1. After 5 days, the media was replaced with fresh media containing tritiated thymidine (^{3}H-thymidine; PerkinElmer, catalog no. NET027E001MC) at a concentration of 1 μCi/mL. After an additional 18 hours of incubation, cells were harvested onto filters using a cell harvester (Tomtec) and incorporation of radiolabeled thymidine was counted on a MicroBeta2 microplate reader (PerkinElmer).

Human ovarian tumor histoculture assay

This study was conducted by Farcast Biosciences. Briefly, ovarian tumors were collected at the time of surgical removal under approval from the appropriate Institutional Review Boards or Institutional Ethics Committees and after obtaining written, informed consent from individual donors, following ethical guidelines of U.S Common Rule. Clinical details of the 30 donors, where available, are included in Supplementary Table S2. Tumors were sectioned into approximately 300 μm slices, randomized, and cultured in 48-well, flat-bottom plates in the presence of autologous serum and PBMCs collected from the donors at the time of surgery. Explants were cultured in RPMI1640 medium supplemented with 8% FBS, 1× insulin-transferrin-selenium (catalog no. 41400045), 1× GlutaMAX (catalog no. 35050038), and 1X penicillin/streptomycin (all from Thermo Fisher Scientific). Tumor slices ($n = 3$/donor) were treated with either an isotype-matched anti-KLH control antibody or the anti-ILT3 antibody 16C5 at 65.7 μg/mL (the C_{max} of pembrolizumab at 2 mg/kg) for 72 hours, with the media and antibody refreshed every 24 hours. Culture supernatants were harvested for analysis of secreted cytokines and chemokines by Luminex assay (ProcartaPlex system). At 72 hours, replicate tumor samples were pooled in RNALater (Thermo Fisher Scientific, catalog no. AM7024), and RNA was purified using the Qiagen RNAeasy kit (Qiagen, catalog no. 74004). RNA concentrations were determined on a NanoDrop spectrophotometer, and sample quality was confirmed by Bioanlyzer (Agilent). Gene expression was analyzed on the Nanostring platform using the nCounter Pancancer IO 360 panel (Nanostring, catalog no. PSTD-HIO360-12). RNA (40 ng/sample) was hybridized with the Reporter CodeSet at 65°C for 20 hours, then mixed with the Capture CodeSet and immediately loaded onto nCounter Sprint cartridges (Nanostring, catalog no. 100078). Quality control (QC) analysis, background correction, and normalization were performed using nSolver 4.0 software (Nanostring) with the default settings, and all samples passed the QC check. To evaluate changes in gene expression, a differential expression analysis was performed on the normalized counts from all 30 patient samples (fold change > 1.5, FDR < 0.05) and a principal component analysis (PCA) plot was generated using the prcomp function in the R program (The R Project for Statistical Computing). If the PC1 distance between the isotype control and the anti-ILT3–treated sample was greater than 5.0, that sample was considered a "responder." A second differential expression analysis was then performed on the 10 samples that met that criterion (OT6, OT36, OT31, OT38, OT42, OT52, OT55, OT57, OT58, and OT60), using the same cutoff values for fold change and FDR.

Statistical analysis

All statistical analyses were performed using GraphPad Prism, version 7.0. Detailed statistical methods are provided in the respective figure legends. For all analyses, a $P < 0.05$ was considered significant.

Results

Fibronectin is a functional ligand for ILT3

Gene expression analyses from TCGA and GETx indicates that *ILT3* is significantly upregulated in numerous cancer types compared with the corresponding normal tissues (Supplementary Fig. S1). However, the ligand that engages ILT3 within the TME and renders myeloid cells suppressive is unknown. To identify a cellular source of the functional ILT3 ligand, we screened over 100 cell lines representing different cell types present within the TME (T cells, myeloid cells, and stromal cells) using a reporter cell line expressing the ILT3 ECD fused to the transmembrane region of PILRβ, which pairs with the signaling adaptor DAP12. Upon ligand binding to ILT3, the immunoreceptor tyrosine-based activation motif (ITAM) of DAP12 drives the GFP reporter gene expression through an NFAT-response promoter (ref. 22; **Fig. 1A**). Although the myeloid and T cell–derived cell lines failed to induce reporter gene activity, LX-2 cells (a fibrogenic human hepatic stellate cell line) treated with TGFβ robustly activated the ILT3-GFP reporter cells (**Fig. 1B**). To confirm the specificity of this interaction, the binding of ILT3-Fc to LX-2 cells was compared with that of a control protein, B7-H4-Fc, by immunofluorescence. ILT3-Fc, but not B7-H4-Fc, bound to TGFβ-treated LX-2 cells (**Fig. 1C**).

To identify the ILT3 binding partner expressed by LX-2 cells, total cell lysate from basal or TGFβ-treated LX-2 cells was affinity-purified with ILT3-Fc or a control Fc protein. A unique band at approximately 260 kDa was identified in the ILT3 pulldown lanes, but not the control

(*Continued.*) The arrow denotes a unique band that is present in the ILT3-Fc pulldown from TGFβ-treated LX-2 cells (independent experiments = 3). **E,** ILT3-GFP reporter cells were cocultured with wild-type (WT) or fibronectin knockout (KO) LX-2 cells with or without pretreatment with TGFβ. GFP expression was determined by flow cytometry, and activation was measured by the percentage of GFP$^+$ reporter cells, reported as the fold change relative to ILT3 reporter cells alone. Statistical significance was assessed by ANOVA combined with Tukey multiple comparison tests ($n = 3$ replicates; independent experiments = 2). **F,** Immunofluorescence staining of TGFβ-treated wild-type LX-2 cells and fibronectin knockout LX-2 cells with a fibronectin antibody (green) or ILT3-Fc (red) using 20× magnification (independent experiments = 3). **G,** ILT3-GFP reporter cells were cultured on the indicated immobilized proteins. The percentage of GFP$^+$ cells was determined by flow cytometry and reported as the fold change relative to unstimulated control cells. Statistical significance was assessed by ANOVA combined with Tukey multiple comparison tests ($n = 3$; independent experiments = 5). **H,** Surface plasmon resonance sensograms of ILT3-Fc and LAIR1-Fc binding to a fibronectin-immobilized surface or a collagen-immobilized surface (independent experiments = 3). *, $P < 0.05$; **, $P < 0.01$; ***, $P < 0.001$; ****, $P < 0.0001$.

Fc lanes, on a silver-stained gel (**Fig. 1D**, arrow). The band was identified by MS as fibronectin, which was enriched 20-fold in the ILT3 pulldown compared with the control pulldown (306 vs. 15 peptides; Supplementary Table S3). To confirm fibronectin as the ligand recognized by ILT3 on LX-2 cells, fibronectin was deleted from LX-2 cells by CRISPR/Cas9-based gene editing, and activation of the ILT3 reporter cells was tested (**Fig. 1E**; Supplementary Fig. S2). Only TGFβ-treated wild-type LX-2 cells were capable of inducing reporter cell activity. For further confirmation, immunofluorescence on both wild-type and fibronectin knockout LX-2 cells was performed. In wild-type LX-2 cells, fibronectin antibody staining largely colocalized with ILT3-Fc staining (**Fig. 1F**, top), whereas in fibronectin knockout cells, binding of both fibronectin antibody and ILT3-Fc to the LX-2 cells was lost (**Fig. 1F**, bottom). Immobilized, but not soluble fibronectin, activated the ILT3-GFP reporter cells in a dose-dependent manner (Supplementary Fig. S3). Although immobilized plasma fibronectin, recombinant fibronectin, and ApoE, a previously described ILT3 binding partner (20), activated the ILT3 reporter cells, the ECM proteins collagen and laminin did not (**Fig. 1G**). To demonstrate a direct protein–protein interaction, ILT3-Fc binding to fibronectin was evaluated by surface plasmon resonance. ILT3 bound specifically to fibronectin, but not collagen, whereas a related collagen receptor, LAIR1 (28), bound only to collagen and not to fibronectin (**Fig. 1H**). Taken together, these data demonstrate that fibronectin is a binding partner for ILT3.

Fibronectin, a structural constituent of the ECM, interacts with numerous molecules, including integrins, heparin, collagen/gelatin, and fibrin, to mediate cellular adhesion, migration, and differentiation (29). Because ILT3 is an ITIM-containing receptor, we asked whether fibronectin could be a signaling ligand for ILT3. To this end, we generated a monoclonal ILT3-specific antibody (16C5) that blocks the fibronectin–ILT3 interaction. The antibody binds to ILT3 with high affinity (Kd = 1 nmol/L; **Fig. 2A**), without any cross-reactivity to other LILR family members (Supplementary Fig. S4), and blocked both fibronectin-induced and ApoE-induced activation of ILT3-GFP reporter cells (**Fig. 2B**).

We next took advantage of cross-talk between ILT3 and the Fcγ receptor (FcR), a key myeloid stimulatory receptor, in human THP-1 monocytes, in which FcR signaling can be suppressed by artificially cross-linking ILT3 with antibodies (16). Using IL8 secretion from THP-1 cells as a readout for FcR activation (30), we found that fibronectin inhibited IL8 production, and this inhibition was reversed with the ILT3 antibody 16C5 (**Fig. 2C**). In contrast, although ApoE activated ILT3 reporter cells (ref. 20; **Fig. 1G**), it failed to suppress FcR-driven cytokine production. To further confirm the specificity of the fibronectin–ILT3 interaction, we utilized CRISPR/Cas9-based gene editing to knock out ILT3 from THP-1 monocytes and then reintroduced wild-type ILT3 or a signaling-incompetent version in which the three tyrosine residues in the ITIM domain were mutated to phenylalanines. FcR-driven IL8 production was no longer inhibited by fibronectin in ILT3 knockout THP-1 cells, whereas reintroducing the wild-type ILT3, but not the ITIM-mutant ILT3, restored the responsiveness of the ILT3 knockout THP-1 cells to fibronectin (**Fig. 2D**; Supplementary Fig. S5). These data confirm that fibronectin is a signaling ligand for ILT3 and can modulate the activity of myeloid cells intracellularly, through an ITIM-dependent mechanism.

ILT3 blockade reprograms suppressive myeloid cells

Next, we explored the role of the fibronectin–ILT3 interaction in primary human myeloid cells. High ILT3 expression is a defining feature of tolerogenic DCs, in which ILT3 expression is significantly higher than on moDCs or primary monocytes (ref. 17; Supplementary Fig. S6A). Tolerogenic DCs generated *in vitro* not only have reduced T-cell stimulatory capacity, but also can actively suppress T-cell activation induced by moDCs (Supplementary Fig. S6B and S6C). To investigate whether engagement of ILT3 by fibronectin impacts the ability of DCs to activate T cells, we introduced fibronectin-expressing, TGFβ-treated LX-2 cells into a mixed lymphocyte reaction in which T-cell proliferation was stimulated by allogeneic DCs. The presence of LX-2 cells significantly reduced T-cell proliferation, and this inhibition was reversed by an ILT3 antibody. When fibronectin knockout LX-2 cells were used, the effects of the ILT3 antibody were lost (**Fig. 3A**). These data support that the fibronectin–ILT3 interaction negatively affects the antigen-presenting function of DCs. To evaluate the impact of fibronectin on myeloid cell–intrinsic functions mediated by ILT3, we measured TNFα secretion from primary tolerogenic DCs activated by FcR ligation. Consistent with the suppressive effects of fibronectin in THP-1 cells, the addition of fibronectin dramatically reduced TNFα secretion. The ILT3 antibody, but not a control antibody, fully reversed this inhibition in a dose-dependent manner (**Fig. 3B**). Collectively, these data indicate that the fibronectin–ILT3 interaction polarizes myeloid cells to a more suppressive state, inhibiting both cell-intrinsic functions and T cell–stimulatory capacity, and this is reversed upon ILT3 blockade.

To understand the mechanisms through which fibronectin–ILT3 signaling affects the functional characteristics of myeloid cells, we exposed peripheral blood monocytes to fibronectin and/or anti-ILT3 during *ex vivo* differentiation into tolerogenic DCs. RNA-seq analysis showed that fibronectin alone affected the expression of 129 genes, whereas treatment of tolerogenic DCs with the ILT3 blocking antibody alone, in the absence of exogenously added fibronectin, altered the expression of 382 genes (**Fig. 3C**). Between these single-agent treatment groups, there were 69 genes that were commonly affected by both fibronectin and anti-ILT3, corresponding to 53% of the genes altered by fibronectin and 18% of the genes altered by anti-ILT3. The observation that anti-ILT3 altered divergent genes in the absence of exogenous fibronectin could be due to the direct effects of antibody binding, as has been reported in other systems lacking fibronectin expression (31), or through blockade of as-yet-unknown endogenous ILT3 ligands. Of the 129 fibronectin-responsive genes, 123 (95%) were no longer significantly changed after treatment with the ILT3 antibody, indicating that ILT3 blockade reversed the majority of fibronectin-driven changes in gene expression (**Fig. 3D**). In addition, we identified a large number (563/960; 59%) of genes that were uniquely responsive to anti-ILT3 in cells treated with fibronectin. Moreover, of the 960 genes that were regulated by ILT3 blockade in the presence of fibronectin, only 343 (36%) were also regulated by anti-ILT3 in the absence of fibronectin, indicating that the majority of the effects of the ILT3 antibody resulted from blockade of the ILT3–fibronectin interaction (**Fig. 3C**). These observations suggest that blocking the ILT3–fibronectin interaction can release myeloid cells from a transcriptionally quiescent state imposed by fibronectin.

Among the 960 genes regulated by ILT3 blockade in fibronectin-treated tolerogenic DCs, anti-ILT3 treatment reduced the expression of classical markers of a suppressive myeloid phenotype (*CD163, FOLR2, CD14*) and increased the expression of genes involved in antigen presentation (*CD1B, CD83, THBD, DCSTAMP*), T-cell costimulation (*CD86, CD40, DPP4, TNFSF14*), and T helper 1 cell (T_H1) polarization (*TBX21*; Supplementary Fig. S7A). These changes suggested that ILT3 blockade had increased the stimulatory capacity of tolerogenic DCs, consistent with their increased ability to activate allogeneic T cells in the presence of fibronectin-expressing LX-2 cells

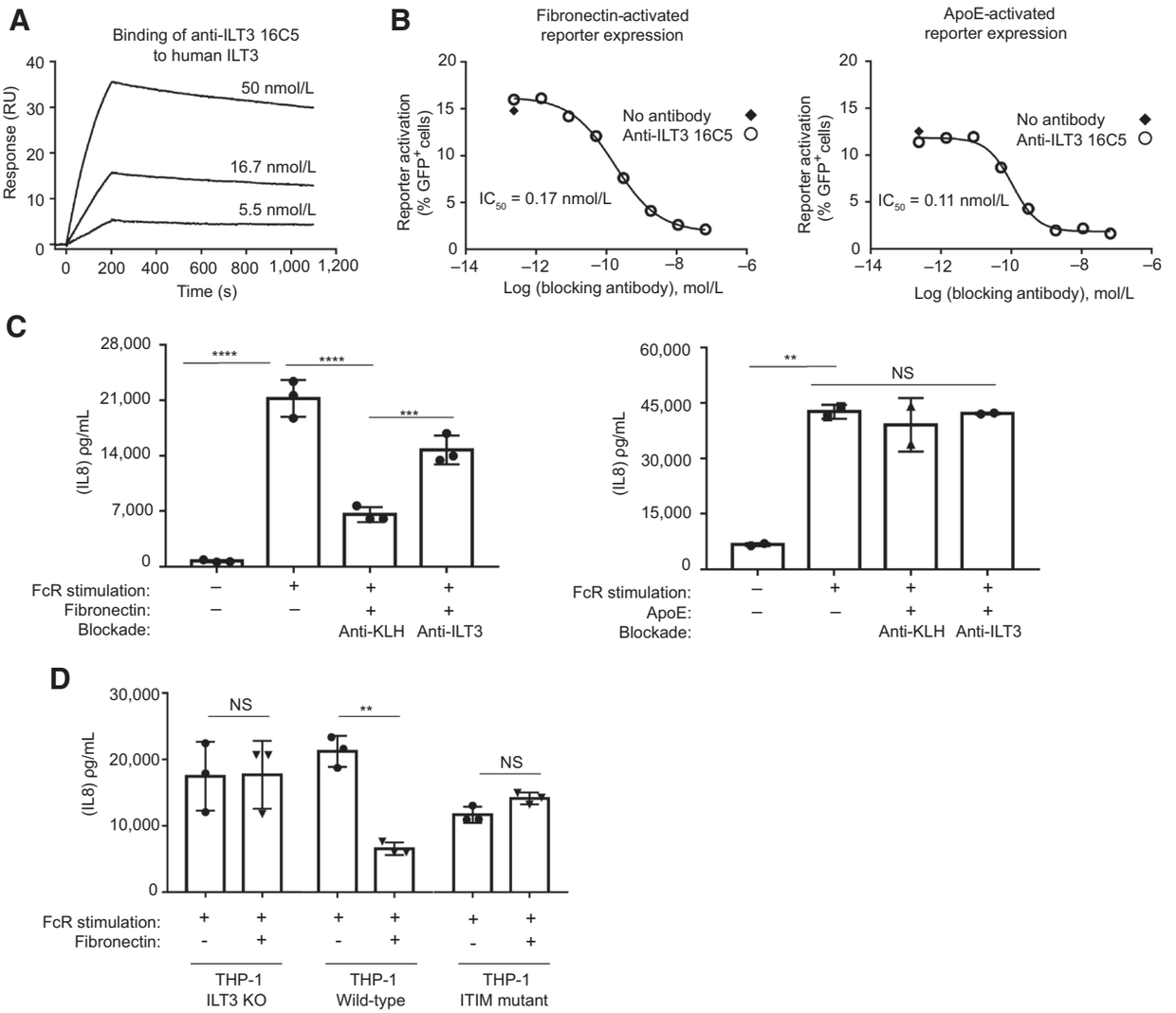

Figure 2.

Fibronectin is a functional ligand for ILT3. **A,** The ILT3 antibody 16C5 binds to human ILT3 by surface plasmon resonance with an affinity of approximately 1 nmol/L at 25°C (independent experiments = 3). **B,** ILT3-GFP reporter cells were cultured on immobilized fibronectin (left) or ApoE (right) in the presence of increasing concentrations of the ILT3 antibody 16C5, and the percentage of GFP^+ cells was measured by flow cytometry. The ILT3 antibody blocked activation of the ILT3 reporter cells by both fibronectin and ApoE, with IC_{50} values of approximately 0.17 and 0.11 nmol/L, respectively (independent experiments = 3). **C,** THP-1 monocytes were grown in tissue cultures plates pretreated with immobilized anti-KLH (as an FcR stimulus), and immobilized fibronectin (left) or ApoE (right) as indicated. Anti-KLH or an ILT3 blocking antibody (16C5) was added in culture media, and IL8 secretion was evaluated after 24 hours. Statistical significance was assessed by ANOVA combined with Tukey multiple comparison tests ($n = 3$ replicates; independent experiments ≥ 5). **D,** In THP-1 cells, ILT3 was knocked out (KO), and then wild-type ILT3 or ITIM-mutated ILT3 was introduced. These cells were subjected to FcR stimulation in the presence or absence of immobilized fibronectin as in **C**. Statistical significance was assessed by ANOVA combined with Tukey multiple comparison tests ($n = 3$ replicates; independent experiments = 3). *, $P < 0.05$; **, $P < 0.01$; ***, $P < 0.001$; ****, $P < 0.0001$. NS, not significant.

(**Fig. 3A**). Gene ontology (GO) analysis of the 960 genes regulated by ILT3 blockade in fibronectin-treated tolerogenic DCs revealed that the biological processes regulated by fibronectin/anti-ILT3 were strongly associated with chemotaxis, migration, and cytokine/chemokine production (Supplementary Table S4). Among the 407 genes annotated as belonging to the GO process of Leukocyte Migration (GO ID 0050900), 73 were differentially expressed in fibronectin-treated tolerogenic DCs treated with anti-ILT3, including *CCL2* [also known as monocyte chemoattractant protein-1 (MCP-1)], *CCL3* [also known as macrophage inflammatory protein-1α (MIP-1α)], *CCL4* (also known as MIP-1β), *CCL5* [also known as regulated upon activation, normal T cell expressed and secreted (RANTES)], CCL22 (also known as monocyte-derived chemokine), and *CSF1* (also known as macrophage/monocyte colony-stimulating factor; **Fig. 3E**; Supplementary Fig. S7B). Analysis of culture supernatants confirmed that fibronectin inhibited the secretion of CCL3 and CCL4 and that ILT3 blockade further enhanced CCL4 secretion (**Fig. 3F**). In addition, DCs in which ILT3 was knocked out via CRISPR/Cas9 secreted a significantly higher level of CCL4 at baseline than control DCs treated with a nontargeting gRNA (**Fig. 3G**; Supplementary Fig. S7C). Fibronectin increased CCL4

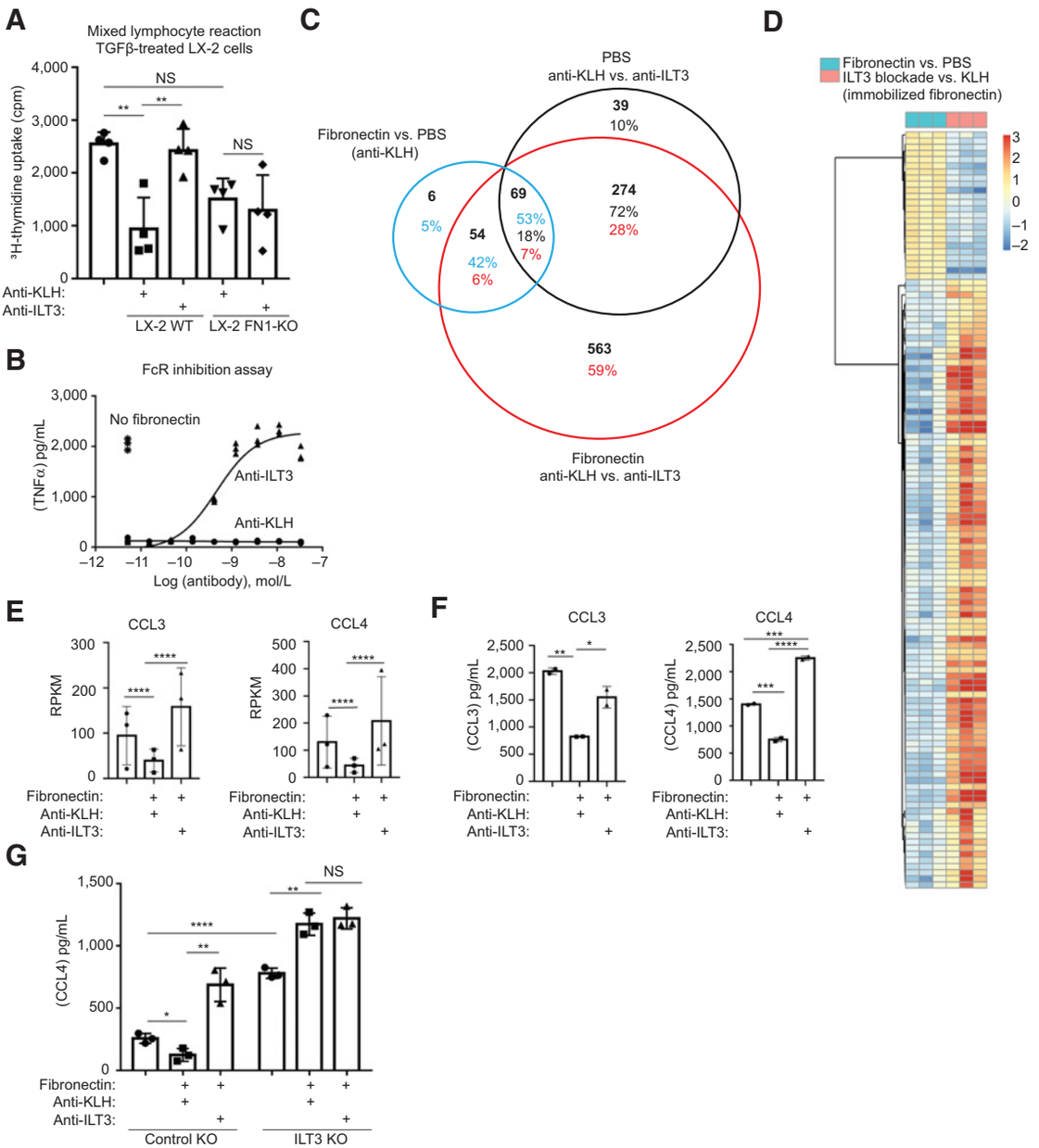

Figure 3.

Blockade of the ILT3–fibronectin interaction reprograms tolerogenic DCs. **A,** T-cell proliferation was measured by ^{3}H-thymidine uptake in a mixed lymphocyte reaction with tolerogenic DCs, allogeneic T cells, and either wild-type (WT) or fibronectin knockout (KO) LX-2 cells pretreated with TGFβ. Statistical significance was assessed by ANOVA combined with Tukey multiple comparison tests ($n = 4$ replicates; independent experiments = 3). **B,** Tolerogenic DCs were stimulated with plate-bound anti-KLH, as an FcR stimulus, in the presence of immobilized fibronectin and increasing doses of soluble ILT3 blocking antibody 16C5, and TNFα secretion was measured ($n = 3$ replicates; independent experiments = 3). **C,** Venn diagram showing overlap among the gene changes induced by fibronectin alone (fibronectin vs. PBS, blue), ILT3 blockade with 16C5 alone (anti-KLH vs. anti-ILT3 on PBS-coated wells, black), and ILT3 blockade in the presence of fibronectin (anti-KLH vs. anti-ILT3 on fibronectin-immobilized wells, red). Genes were considered differentially expressed if the fold change was > 1.5 and the FDR was < 0.05. **D,** Fibronectin-mediated changes reversed by ILT3 blockade with 16C5 in tolerogenic DCs. Heatmap representing the fibronectin-driven changes in gene expression (fibronectin vs. PBS, left) compared with the anti-ILT3–driven changes in gene expression (anti-KLH vs. anti-ILT3 on fibronectin-immobilized wells, right) for the 123 genes that were differentially expressed (fold change > 1.5, FDR < 0.05) in fibronectin-treated tolerogenic DCs compared with PBS-treated tolerogenic DCs. **E,** Changes in the expression of CCL3 and CCL4 by tolerogenic DCs cultured on fibronectin-immobilized wells in the presence or absence of anti-ILT3 16C5. **F,** Secretion of CCL3 (left) and CCL4 (right) by tolerogenic DCs treated with anti-ILT3 16C5 on fibronectin-immobilized wells. Statistical significance was assessed by ANOVA combined with Tukey multiple comparison tests ($n = 2$ replicates; independent experiments = 3, each an individual donor). **G,** CCL4 secretion from primary DCs in which ILT3 was knocked out by CRISPR/Cas9-based gene editing. Control DCs were treated with a scrambled gRNA. Statistical significance was calculated by unpaired *t* tests ($n = 3$ replicates; independent experiments = 3). Gene expression data represent the mean ± SEM of three donors analyzed in the RNA-seq experiment. *, $P < 0.05$; **, $P < 0.01$; ***, $P < 0.001$; ****, $P < 0.0001$. NS, not significant.

secretion from the ILT3 knockout cells, rather than inhibiting it, perhaps through engagement of other fibronectin-binding receptors such as integrins (32). Nevertheless, ILT3 knockout DCs no longer responded to the ILT3 antibody, confirming the dominant role of the fibronectin–ILT3 axis in regulating chemokine secretion by DCs and suggesting that fibronectin could inhibit immune-cell trafficking to sites of inflammation by modulating myeloid cell chemokine production via ILT3. Collectively, these results suggest that blocking the ILT3–fibronectin interaction can release myeloid cells from a transcriptionally quiescent and functionally suppressed state imposed by fibronectin.

To study the signal transduction of the fibronectin–ILT3 interaction in primary human immune cells, we first investigated the contribution of the tyrosine phosphatases SHP1 and SHP2, two key immune modulators that are recruited to the ITIM-domain of immune suppressive receptors (33). Using CRISPR/Cas9 gene editing to knockout SHP1 or SHP2 in tolerogenic DCs, we found that loss of SHP1 ablated the inhibitory effect of fibronectin on CCL4 secretion, whereas loss of SHP2 had no effect (**Fig. 4A** and **B**; Supplementary Fig. S7C). Furthermore, we investigated the involvement of the tyrosine kinase SYK, which plays a role in limiting the development of DCs into a "regulatory" phenotype that suppresses inflammation in a mouse colitis model (34). Loss of SYK completely ablated CCL4 secretion (**Fig. 4C**; Supplementary Fig. S7C). These data demonstrate that SHP1 is a major ILT3-associated phosphatase regulating chemokine secretion by fibronectin-treated DCs through inhibition of SYK.

Therapeutic potential of ILT3 blockade

Although it is well-documented that stroma-rich tumors are associated with poor outcomes to immunotherapy (8), the cause of this phenomenon remains unclear. Our results provide a potential explanation for this in that they suggest that chemokine secretion from tumor-associated myeloid cells is inhibited by the fibronectin–ILT3 interaction. To examine this possibility, we used a tumor histoculture system, in which 30 human ovarian tumor specimens and matched patient immune cells were cocultured *ex vivo* in the presence of anti-ILT3 or an isotype-matched control antibody. Culture supernatants were harvested for analysis of chemokine and cytokine secretion, and explants were harvested for gene expression analysis by Nanostring using the immune oncology–focused, 770-gene Pancancer IO 360 gene expression panel. PCA identified a subset of 10 patient samples that "responded" to anti-ILT3 treatment (**Fig. 5A** and **B**). Although the limited size of the gene expression panel prevented us from conducting pathway analyses of the differentially expressed genes, we did observe decreased levels of classical markers of a protumor myeloid cell phenotype (*CD163, MRC1, CD36*) and increased levels of a marker of an antitumor phenotype (*NOS2*) in the anti-ILT3–treated tumors (ref. 35; **Fig. 5C**). We did not detect any cytokine changes suggestive of an adaptive immune response as the T cell–derived cytokines that were measured, including IL2, TNFα, and IFNγ, were undetectable or unaffected by the anti-ILT3 treatment. Nevertheless, these data indicate that ILT3 blockade can reprogram suppressive myeloid cells within human tumors.

To confirm this observation, we turned to TCGA dataset and analyzed the expression levels of *CD163, MRC1*, and *CD36* in ovarian tumor samples with high ILT3 expression (*NOS2* was excluded because its expression level was exceedingly low in all samples, with a median FPKM of 0.06). We found that these three genes were significantly more highly expressed in samples with high fibronectin expression, compared with samples with low fibronectin expression. This effect appears to be ILT3 dependent, as the differential expression associated with fibronectin levels was lost in samples with low ILT3 expression (**Fig. 5D**). The expression profile of these protumor myeloid cell genes in primary human ovarian tumors is consistent with an ILT3-mediated effect of fibronectin as demonstrated in the histoculture study. Finally, multiplex cytokine/chemokine analysis of all samples revealed that ILT3 blockade significantly increased the production of CCL3, CCL4, IL8, CCL5, and CXCL10 (**Fig. 5E**). Taken together, these data highlight the promise of fibronectin–ILT3 blockade as a therapeutic strategy to reprogram suppressive myeloid cells and enhance immune-cell recruitment into the immune-excluded TME.

Discussion

In this study, we identified fibronectin as a ligand for ILT3 and demonstrated that this ligand–receptor interaction polarized human myeloid cells to a suppressive state. To our knowledge, this is the first time that a bona fide ILT3 ligand has been found to exert a functional effect on ILT3-expressing primary, nonmalignant human immune cells. CD166 is reported to bind ILT3-Fc; however, this interaction inhibits the homophilic interaction of CD166 between malignant cells,

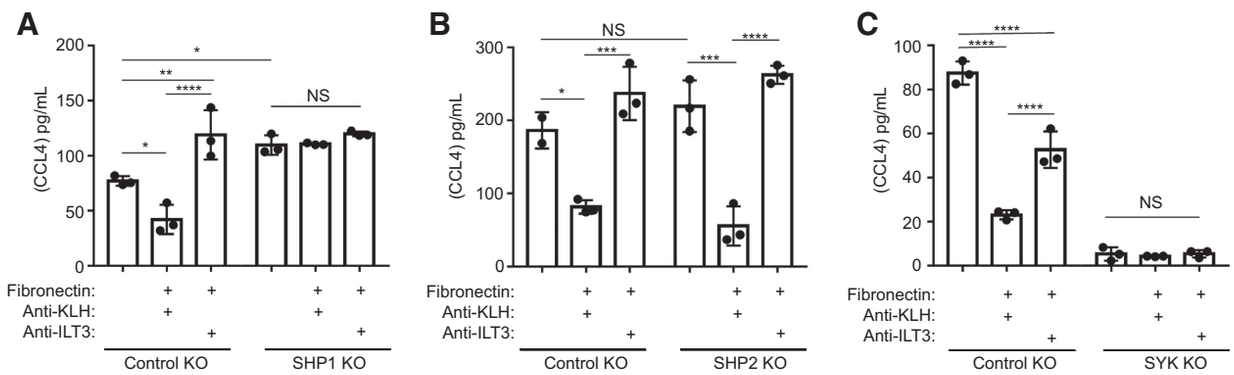

Figure 4.

Fibronectin suppresses SYK-driven chemokine production in tolerogenic DCs via SHP1. Primary DCs subjected to CRISPR/Cas9 knockout with scrambled (control), SHP1 (**A**), SHP2 (**B**), or SYK (**C**) gRNAs were cultured for 5 days in the presence of immobilized fibronectin and the ILT3 antibody 16C5 or control KLH antibody as indicated. CCL4 secretion in the culture supernatant was measured by Luminex assay. Statistical significance was assessed by ANOVA combined with Tukey multiple comparison tests ($n = 3$ replicates; independent experiments = 3). *, $P < 0.05$; **, $P < 0.01$; ***, $P < 0.001$; ****, $P < 0.0001$. KO, knockout; NS, not significant.

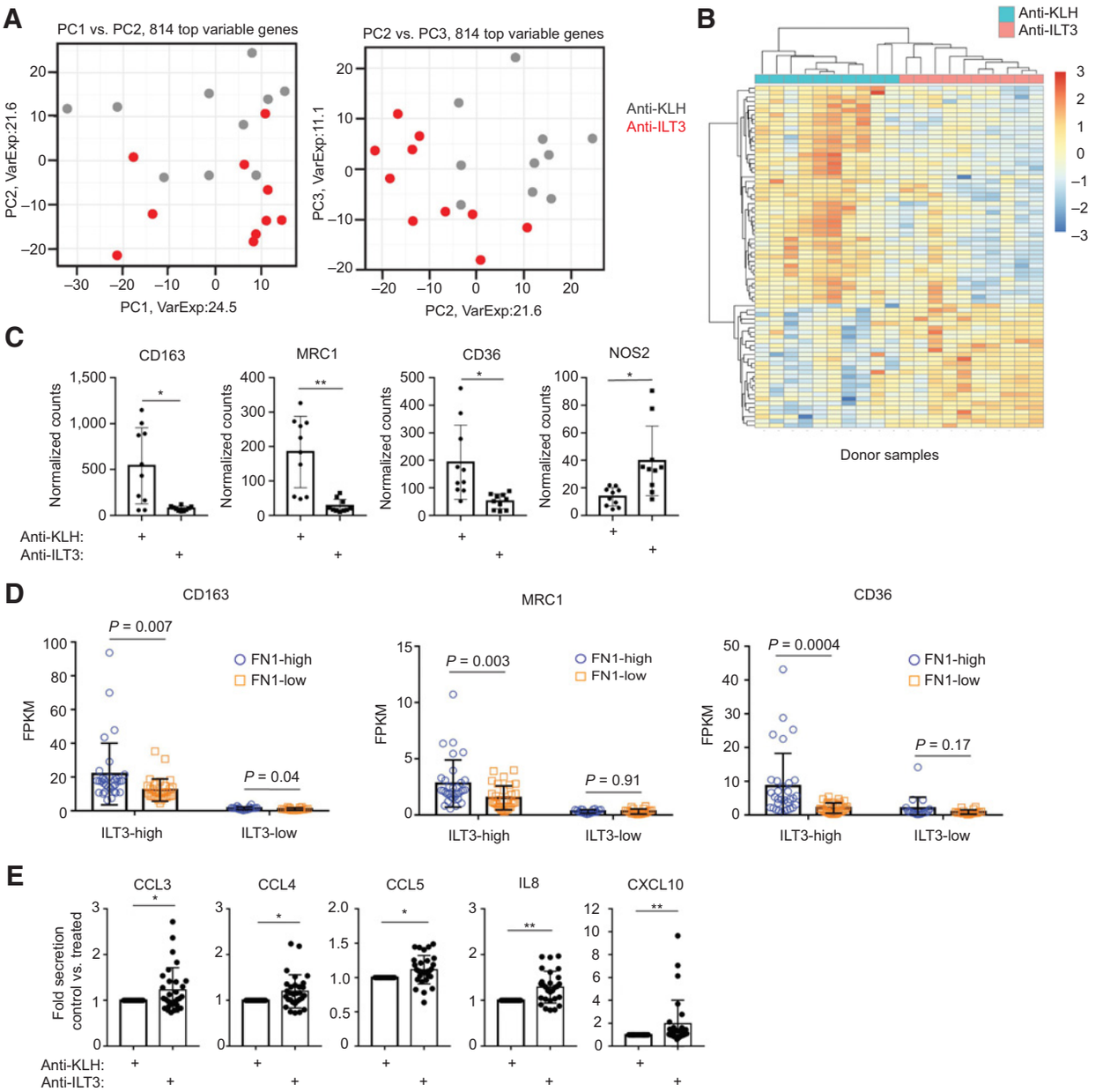

Figure 5.

The ILT3–fibronectin interaction contributes to myeloid-cell suppression in primary human tumors. Human ovarian tumor explants were cultured in media containing anti-KLH or anti-ILT3 16C5. After 72 hours, tissue explants were harvested into RNALater and gene expression was analyzed by Nanostring nCounter gene expression assay using the Pancancer IO 360 panel. **A,** PCA of 10 patients in which the PC1 distance between the anti-KLH–treated sample and the matched anti-ILT3–treated sample was > 5.0. **B,** Heatmap of the differentially expressed genes (fold change > 1.5; FDR < 0.05) in the 10 "responding" patients. **C,** A subset analysis of the 10 patients classified as ILT3 "responders" revealed changes in multiple genes associated with myeloid cell polarization upon anti-ILT3 treatment. **D,** Gene expression data were extracted from 422 primary ovarian tumor samples from TCGA. Samples were first divided into ILT3-low (FPKM < 2, $n = 71$, ~17% of samples) and ILT3-high (FPKM > 10, $n = 128$, ~30% of samples) groups. Within each group, the gene expression of CD163, MRC1, and CD36 in the samples with the lowest 25% of FN1 expression (FN1-low) and those with the highest 25% (FN1-high) were analyzed and plotted. Statistical significance was assessed using two-tailed Student *t* tests. **E,** Culture supernatants from the explants were analyzed for cytokine/chemokine content by Luminex. IL8 was measured from samples taken after 24 hours incubation, whereas CCL3, CCL4, CCL5, and CXCL10 were measured after 72 hours incubation. Statistical significance was assessed using paired two-tailed *t* tests. *, $P < 0.05$; **, $P < 0.01$; ***, $P < 0.001$; ****, $P < 0.0001$.

rather than having a functional effect on ILT3-expressing cells (19). Recently, Deng and colleagues discovered ApoE as a ligand for ILT3 by screening human and mouse serum using ILT3 reporter cells (20). Although we were able to confirm this interaction, there are notable differences between the ApoE–ILT3 and fibronectin–ILT3 ligand–receptor pairs. For example, engagement of ILT3 on myeloid cells by fibronectin resulted in SYK inhibition via SHP1 recruitment, whereas ApoE–ILT3 signals through the IKKα/β pathway by SHP2

recruitment in leukemia cells but has no effect on nonmalignant myeloid cells (20). ILT3 is expressed ectopically on some cancer cells (13, 36, 37). The ApoE–ILT3 interaction on non–small cell lung cancer cells activates ERK1/2 signaling and results in epithelial–mesenchymal transition and increased VEGF-A expression (37). These diverse responses of ILT3 to its ligands suggest that additional factors are likely involved in a cell-type specific manner to govern the biological outcome of ILT3 engagement.

The ability of the fibronectin–ILT3 interaction to suppress SYK kinase, a crucial regulator of numerous aspects of myeloid cell biology (38), suggests that this interaction has the potential to broadly affect myeloid cell function. Of note, SYK is critical for sustained leukocyte adhesion *in vivo* (39). Mechanistically, SYK mediates integrin signaling through association with the ITAM-containing immune adapter proteins DAP12 and FcRγ (40). Because fibronectin is a well-established ligand for integrins, it is conceivable that ILT3, by sharing the same ligand, could also be involved in the regulation of integrin biology. An emerging concept in immunology is that of "paired receptors," in which inhibitory and stimulatory receptors share a common ligand to balance the immunologic response (41). Dissecting the functional outcome of engaging both integrin and ILT3 will be important to elucidate whether there is a functional cross-talk between these two pathways.

Over the past decade, immune checkpoint inhibitors that target inhibitory receptors on T cells have transformed the clinical oncology landscape. Antibodies targeting CTL-associated protein (CTLA)-4 or the PD-1/PD-L1 axis are now approved as first- or second-line therapies, alone or in combination with cytotoxic chemotherapy, in numerous tumor types (42). Despite these tremendous clinical successes, only a minority of patients achieve durable clinical responses to T-cell checkpoint inhibitors. There is therefore significant interest in combining immune checkpoint inhibitors with agents that target other mechanisms of immunosuppression within the TME. Stroma and suppressive myeloid cells are recognized as elements within the TME contributing to the inhibition of antitumor T-cell responses (43). Notably, ILT3-mediated immunosuppression appears to be a clinically relevant mechanism inhibiting antitumor immunity, as myeloid cell expression of ILT3 is increased in patients with melanoma that fail to respond to immune checkpoint inhibitors (44).

Numerous studies of the response to immune checkpoint inhibitors indicate that the density of intratumoral T cells is a strong predictor of patient survival (45, 46). In addition to their better-known role in antigen presentation, DCs can influence adaptive immune responses by recruiting T cells to sites of inflammation through their secretion of T cell–recruiting chemokines (47, 48). Primed effector T cells upregulate the chemokine receptors CCR2, CCR5, and CXCR3, which promote their infiltration into infected tissue in response to DC-derived chemokines including CCL3, CCL4, CCL5, and CXCL10 (49). DC-derived CXCL10, in particular, is critical for recruitment of $CD8^+$ T cells into the TME, as genetic ablation of $CD103^+$ DCs reduces the production of CXCL10 and impairs effector $CD8^+$ T-cell infiltration in a murine melanoma model (47). In human colorectal tumors, expression of ILT3 inversely correlates with the density of intratumoral $CD45RO^+$ memory T cells (13), suggesting that tolerogenic DCs may have impaired ability to produce T cell–recruiting chemokines and directly linking ILT3 to T-cell exclusion. Our findings suggest that suppressed chemokine production may be a general feature of tolerogenic DCs and highlight a role for DCs in coordinating the adaptive immune response via chemokine production.

Because stromal-dependent immune suppression is a substantial barrier to immunotherapy efficacy, developing strategies to target stromal-mediated immunosuppression is an attractive therapeutic approach. Our work identifies the fibronectin–ILT3 interaction as a pathway through which the ECM directly promotes myeloid cell suppression within the TME. As ILT3 is a member of the leukocyte immunoglobulin like receptor (LILR) family, which also includes the collagen receptor LAIR1, it is intriguing to speculate that this family of inhibitory receptors may have evolved to induce tolerance through interactions with the ECM. Although these receptor–ligand interactions have been co-opted as mechanisms of immune suppression in cancer, they may regulate immune homeostasis in other compartments such as the bone marrow, in which ECM proteins form specialized niches that regulate immune-cell expansion and maturation (50). The LILR family of receptors may thus represent the next wave of myeloid cell–expressed immune checkpoint inhibitors, analogous to the B7 family of molecules that regulate T-cell immunosuppression. By blocking the "stromal checkpoint" represented by the fibronectin–ILT3 interaction, it may be possible to reprogram tumor-associated myeloid cells to a more stimulatory phenotype, enhancing T-cell infiltration and activation within the TME and increasing responses to immune checkpoint blockade.

Authors' Disclosures

K.J. Paavola reports other support from Merck during the conduct of the study, as well as a patent for PCT/US2020/065642 pending. J.M. Roda reports other support from Merck during the conduct of the study, as well as a patent for PCT/US2020/065642 pending. V.Y. Lin reports other support from Merck during the conduct of the study, as well as a patent for PCT/US2020/065642 pending. P. Chen reports other support from NGM Biopharmaceuticals during the conduct of the study. K.P. O'Hollaren reports other support from Merck during the conduct of the study. R. Ventura reports other support from Merck during the conduct of the study. S.C. Crawley reports other support from Merck during the conduct of the study, as well as a patent for PCT/US2020/065642 pending. B. Li reports other support from Merck during the conduct of the study, as well as a patent for PCT/US2020/065642 pending. H.-I.H. Chen reports other support from Merck during the conduct of the study. S. Malmersjö reports other support from NGM Biopharmaceuticals and Merck during the conduct of the study, as well as a patent for PCT/US2020/065642 pending. G. Horner reports that NGM Biopharmaceuticals received funding for this program from Merck under a collaboration agreement between the parties. W. Guo reports other support from Merck during the conduct of the study. A.K. Kutach reports other support from Merck during the conduct of the study. K. Mondal reports other support from NGM Biopharmaceuticals during the conduct of the study. Z. Zhang reports other support from NGM Biopharmaceuticals during the conduct of the study. J.S. Lichtman reports other support from Merck during the conduct of the study, and is a shareholder in NGM Biopharmaceuticals. C. Song reports other support from NGM Biopharmaceuticals during the conduct of the study. L.B. Rivera reports other support from Merck during the conduct of the study. W. Liu reports other support from Merck during the conduct of the study. J. Luo reports other support from NGM Biopharmaceuticals during the conduct of the study. Y. Wang reports a patent for PCT/US2020/065642 pending. M.J. Solloway reports other support from Merck during the conduct of the study. B.B. Allan reports other support from NGM Biopharmaceuticals during the conduct of the study. A. Kekatpure reports other support from Merck during the conduct of the study. S.R. Starck reports other support from NGM Biopharmaceuticals, which received funding for this program from Merck under a collaboration agreement between the parties, during the conduct of the study. B. Fan reports other support from Merck during the conduct of the study. C. Chu reports other support from NGM Biopharmaceuticals during the conduct of the study. M. Molgora reports other support from NGM Biopharmaceuticals during the conduct of the study. M. Colonna reports grants from NGM Biopharmaceuticals during the conduct of the study. D.D. Kaplan reports a patent for ILT3 binding agents pending, and is an employee and stockholder of NGM Biopharmaceuticals. J.-Y. Hsu reports other support from Merck during the conduct of the study, as well as a patent for PCT/US2020/065642 pending. No disclosures were reported by the other authors.

Authors' Contributions

K.J. Paavola: Investigation, writing–original draft, writing–review and editing. **J.M. Roda:** Investigation, writing–original draft, writing–review and editing. **V.Y. Lin:** Investigation. **P. Chen:** Investigation. **K.P. O'Hollaren:** Investigation. **R. Ventura:** Investigation. **S.C. Crawley:** Investigation. **B. Li:** Resources. **H.-I.H. Chen:** Data curation, formal analysis. **S. Malmersjö:** Investigation. **N.A. Sharkov:** Investigation. **G. Horner:** Investigation. **W. Guo:** Resources. **A.K. Kutach:** Resources. **K. Mondal:** Investigation. **Z. Zhang:** Resources. **J.S. Lichtman:** Resources, data curation, formal analysis. **C. Song:** Investigation. **L.B. Rivera:** Resources. **W. Liu:** Resources. **J. Luo:** Resources. **Y. Wang:** Resources, supervision. **M.J. Solloway:** Resources. **B.B. Allan:** Supervision. **A. Kekatpure:** Resources. **S.R. Starck:** Resources. **R. Haldankar:** Resources. **B. Fan:** Resources. **C. Chu:** Resources. **J. Tang:** Resources. **M. Molgora:** Resources. **M. Colonna:** Supervision, writing–review and editing. **D.D. Kaplan:** Conceptualization, supervision. **J.-Y. Hsu:** Conceptualization, supervision, writing–original draft, writing–review and editing.

Acknowledgments

The authors thank Lewis Lanier for providing the CT237 reporter cell line; Richard Yan for anti-ILT3 antibody production; Mehrdad Moshrefi and Keith Akama for control antibody and fibronectin production; Yiyuan Yi for hybridoma sequencing; and Raymond Li, Jing Zhou, and Jared Higbee for LAIR1-Fc production. They thank Jeong Kim, Jon Sitrin, and Geoffrey Stone for critical reading of the article and Jeong Kim and Jiping Zha for sharing unpublished data that are informative to this work.

This work was supported by NGM Biopharmaceuticals.

The costs of publication of this article were defrayed in part by the payment of page charges. This article must therefore be hereby marked *advertisement* in accordance with 18 U.S.C. Section 1734 solely to indicate this fact.

Received March 27, 2021; revised June 9, 2021; accepted August 17, 2021; published first August 23, 2021.

References

1. Ren Q, Zhu P, Zhang H, Ye T, Liu D, Gong Z, et al. Identification and validation of stromal-tumor microenvironment-based subtypes tightly associated with PD-1/PD-L1 immunotherapy and outcomes in patients with gastric cancer. Cancer Cell Int 2020;20:92.
2. Chakravarthy A, Khan L, Bensler NP, Bose P, De Carvalho DD. TGF-beta-associated extracellular matrix genes link cancer-associated fibroblasts to immune evasion and immunotherapy failure. Nat Commun 2018;9:4692.
3. Wang L, Saci A, Szabo PM, Chasalow SD, Castillo-Martin M, Domingo-Domenech J, et al. EMT- and stroma-related gene expression and resistance to PD-1 blockade in urothelial cancer. Nat Commun 2018;9:3503.
4. Salmon H, Franciszkiewicz K, Damotte D, Dieu-Nosjean MC, Validire P, Trautmann A, et al. Matrix architecture defines the preferential localization and migration of T cells into the stroma of human lung tumors. J Clin Invest 2012;122:899–910.
5. Salmon H, Donnadieu E. Within tumors, interactions between T cells and tumor cells are impeded by the extracellular matrix. Oncoimmunology 2012;1:992–4.
6. Wen Y, Wang CT, Ma TT, Li ZY, Zhou LN, Mu B, et al. Immunotherapy targeting fibroblast activation protein inhibits tumor growth and increases survival in a murine colon cancer model. Cancer Sci 2010;101:2325–32.
7. Peng DH, Rodriguez BL, Diao L, Chen L, Wang J, Byers LA, et al. Collagen promotes anti-PD-1/PD-L1 resistance in cancer through LAIR1-dependent CD8(+) T cell exhaustion. Nat Commun 2020;11:4520.
8. Mariathasan S, Turley SJ, Nickles D, Castiglioni A, Yuen K, Wang Y, et al. TGFbeta attenuates tumour response to PD-L1 blockade by contributing to exclusion of T cells. Nature 2018;554:544–8.
9. Chen DS, Mellman I. Oncology meets immunology: the cancer-immunity cycle. Immunity 2013;39:1–10.
10. Chu CC, Ali N, Karagiannis P, Di Meglio P, Skowera A, Napolitano L, et al. Resident CD141 (BDCA3)+ dendritic cells in human skin produce IL-10 and induce regulatory T cells that suppress skin inflammation. J Exp Med 2012;209:935–45.
11. Ghiringhelli F, Puig PE, Roux S, Parcellier A, Schmitt E, Solary E, et al. Tumor cells convert immature myeloid dendritic cells into TGF-beta-secreting cells inducing CD4+CD25+ regulatory T cell proliferation. J Exp Med 2005;202:919–29.
12. DeVito NC, Plebanek MP, Theivanthiran B, Hanks BA. Role of tumor-mediated dendritic cell tolerization in immune evasion. Front Immunol 2019;10:2876.
13. Liu J, Lu CX, Zhang F, Lv W, Liu C. Expression of ILT3 predicts poor prognosis and is inversely associated with infiltration of CD45RO+ T cells in patients with colorectal cancer. Pathol Res Pract 2018;214:1621–5.
14. Treilleux I, Blay JY, Bendriss-Vermare N, Ray-Coquard I, Bachelot T, Guastalla JP, et al. Dendritic cell infiltration and prognosis of early stage breast cancer. Clin Cancer Res 2004;10:7466–74.
15. Scarlett UK, Rutkowski MR, Rauwerdink AM, Fields J, Escovar-Fadul X, Baird J, et al. Ovarian cancer progression is controlled by phenotypic changes in dendritic cells. J Exp Med 2012;209:495–506.
16. Cella M, Dohring C, Samaridis J, Dessing M, Brockhaus M, Lanzavecchia A, et al. A novel inhibitory receptor (ILT3) expressed on monocytes, macrophages, and dendritic cells involved in antigen processing. J Exp Med 1997;185:1743–51.
17. Manavalan JS, Rossi PC, Vlad G, Piazza F, Yarilina A, Cortesini R, et al. High expression of ILT3 and ILT4 is a general feature of tolerogenic dendritic cells. Transpl Immunol 2003;11:245–58.
18. Malinarich F, Duan K, Hamid RA, Bijin A, Lin WX, Poidinger M, et al. High mitochondrial respiration and glycolytic capacity represent a metabolic phenotype of human tolerogenic dendritic cells. J Immunol 2015;194:5174–86.
19. Xu Z, Chang CC, Li M, Zhang QY, Vasilescu EM, D'Agati V, et al. ILT3.Fc-CD166 interaction induces inactivation of p70 S6 kinase and inhibits tumor cell growth. J Immunol 2018;200:1207–19.
20. Deng M, Gui X, Kim J, Xie L, Chen W, Li Z, et al. LILRB4 signalling in leukaemia cells mediates T cell suppression and tumour infiltration. Nature 2018;562:605–9.
21. Verschueren E, Husain B, Yuen K, Sun Y, Paduchuri S, Senbabaoglu Y, et al. The immunoglobulin superfamily receptome defines cancer-relevant networks associated with clinical outcome. Cell 2020;182:329–44.
22. Arase H, Mocarski ES, Campbell AE, Hill AB, Lanier LL. Direct recognition of cytomegalovirus by activating and inhibitory NK cell receptors. Science 2002;296:1323–6.
23. Hu J, Ge H, Newman M, Liu K. OSA: a fast and accurate alignment tool for RNA-Seq. Bioinformatics 2012;28:1933–4.
24. Li B, Ruotti V, Stewart RM, Thomson JA, Dewey CN. RNA-Seq gene expression estimation with read mapping uncertainty. Bioinformatics 2010;26:493–500.
25. von Boehmer L, Liu C, Ackerman S, Gitlin AD, Wang Q, Gazumyan A, et al. Sequencing and cloning of antigen-specific antibodies from mouse memory B cells. Nat Protoc 2016;11:1908–23.
26. Robinson MD, McCarthy DJ, Smyth GK. edgeR: a Bioconductor package for differential expression analysis of digital gene expression data. Bioinformatics 2010;26:139–40.
27. McCarthy DJ, Chen Y, Smyth GK. Differential expression analysis of multifactor RNA-Seq experiments with respect to biological variation. Nucleic Acids Res 2012;40:4288–97.
28. Lebbink RJ, de Ruiter T, Adelmeijer J, Brenkman AB, van Helvoort JM, Koch M, et al. Collagens are functional, high affinity ligands for the inhibitory immune receptor LAIR-1. J Exp Med 2006;203:1419–25.
29. Pankov R, Yamada KM. Fibronectin at a glance. J Cell Sci 2002;115:3861–3.
30. Marsh CB, Anderson CL, Lowe MP, Wewers MD. Monocyte IL-8 release is induced by two independent Fc gamma R-mediated pathways. J Immunol 1996;157:2632–7.
31. Singh L, Muise ES, Bhattacharya A, Grein J, Javaid S, Stivers P, et al. ILT3 (LILRB4) promotes the immunosuppressive function of tumor-educated human monocytic myeloid-derived suppressor cells. Mol Cancer Res 2021;19:702–16.
32. Rezzonico R, Imbert V, Chicheportiche R, Dayer JM. Ligation of CD11b and CD11c beta(2) integrins by antibodies or soluble CD23 induces macrophage inflammatory protein 1alpha (MIP-1alpha) and MIP-1beta production in primary human monocytes through a pathway dependent on nuclear factor-kappaB. Blood 2001;97:2932–40.
33. Garg M, Wahid M, Khan FD. Regulation of peripheral and central immunity: understanding the role of Src homology 2 domain-containing tyrosine phosphatases, SHP-1 & SHP-2. Immunobiology 2020;225:151847.
34. Hang L, Blum AM, Kumar S, Urban JF Jr, Mitreva M, Geary TG, et al. Downregulation of the Syk signaling pathway in intestinal dendritic cells is sufficient to induce dendritic cells that inhibit colitis. J Immunol 2016;197:2948–57.

35. Roszer T. Understanding the mysterious M2 macrophage through activation markers and effector mechanisms. Mediators Inflamm 2015;2015:816460.
36. Zhang Y, Lu N, Xue Y, Zhang M, Li Y, Si Y, et al. Expression of immunoglobulin-like transcript (ILT)2 and ILT3 in human gastric cancer and its clinical significance. Mol Med Rep 2012;5:910–6.
37. Li J, Gao A, Zhang F, Wang S, Wang J, Wang J, et al. ILT3 promotes tumor cell motility and angiogenesis in non-small cell lung cancer. Cancer Lett 2021;501: 263–76.
38. Mocsai A, Ruland J, Tybulewicz VL. The SYK tyrosine kinase: a crucial player in diverse biological functions. Nat Rev Immunol 2010;10:387–402.
39. Frommhold D, Mannigel I, Schymeinsky J, Mocsai A, Poeschl J, Walzog B, et al. Spleen tyrosine kinase Syk is critical for sustained leukocyte adhesion during inflammation in vivo. BMC Immunol 2007;8:31.
40. Mocsai A, Abram CL, Jakus Z, Hu Y, Lanier LL, Lowell CA. Integrin signaling in neutrophils and macrophages uses adaptors containing immunoreceptor tyrosine-based activation motifs. Nat Immunol 2006;7:1326–33.
41. Levi-Schaffer F, Mandelboim O. Inhibitory and coactivating receptors recognising the same ligand: immune homeostasis exploited by pathogens and tumours. Trends Immunol 2018;39:112–22.
42. Xin Yu J, Hubbard-Lucey VM, Tang J. Immuno-oncology drug development goes global. Nat Rev Drug Discov 2019;18:899–900.
43. Jenkins RW, Barbie DA, Flaherty KT. Mechanisms of resistance to immune checkpoint inhibitors. Br J Cancer 2018;118:9–16.
44. Sade-Feldman M, Yizhak K, Bjorgaard SL, Ray JP, de Boer CG, Jenkins RW, et al. Defining T cell states associated with response to checkpoint immunotherapy in melanoma. Cell 2019;176:404.
45. Galon J, Costes A, Sanchez-Cabo F, Kirilovsky A, Mlecnik B, Lagorce-Pages C, et al. Type, density, and location of immune cells within human colorectal tumors predict clinical outcome. Science 2006;313:1960–4.
46. Tumeh PC, Harview CL, Yearley JH, Shintaku IP, Taylor EJ, Robert L, et al. PD-1 blockade induces responses by inhibiting adaptive immune resistance. Nature 2014;515:568–71.
47. Spranger S, Dai D, Horton B, Gajewski TF. Tumor-residing Batf3 dendritic cells are required for effector T cell trafficking and adoptive T cell therapy. Cancer Cell 2017;31:711–23.
48. Thaiss CA, Semmling V, Franken L, Wagner H, Kurts C. Chemokines: a new dendritic cell signal for T cell activation. Front Immunol 2011;2:31.
49. Bromley SK, Mempel TR, Luster AD. Orchestrating the orchestrators: chemokines in control of T cell traffic. Nat Immunol 2008;9:970–80.
50. Sangaletti S, Chiodoni C, Tripodo C, Colombo MP. Common extracellular matrix regulation of myeloid cell activity in the bone marrow and tumor microenvironments. Cancer Immunol Immunother 2017;66:1059–67.